Classical over-the-barrier model for neutralization of highly charged ions above thin dielectric films

R. E. Lake,[1,2,*] C. E. Sosolik,[2] and J. M. Pomeroy[1]
[1]*National Institute of Standards and Technology, Gaithersburg, Maryland 20899, USA*
[2]*Department of Physics and Astronomy, Clemson University, Clemson, South Carolina 29634, USA*
(Received 3 January 2013; published 3 June 2013)

We apply the classical over-the-barrier (COB) model to charge transfer between highly charged ions (HCIs) and targets consisting of thin dielectric films on metals. Distances for the onset of classically allowed above-surface electron capture are obtained as a function of HCI charge state, film thickness, film permittivity, and film-metal electron binding energies. The model describes the crossover between the previously existing COB model for bulk metals and bulk dielectrics as the thickness of a dielectric film on a metal substrate increases through three distinct regimes. For ultrathin films with low permittivity and positive electron affinity, over-the-barrier charge transfer initiates from the metal electrons behind the film and critical distances are greater than those from bare metal targets. This result is consistent and compared with the recent observation of potential emission enhancement above thin C_{60} films on Au(111) with increasing film thickness [Bodewits, Hoekstra, Kowarik, Dobes, and Aumayr, Phys. Rev. A **84**, 042901 (2011)].

DOI: 10.1103/PhysRevA.87.062901 PACS number(s): 34.35.+a, 34.70.+e, 79.20.Rf

I. INTRODUCTION

Slow highly charged ion (HCI) interactions with solids continues to be an active area of research at the interface of condensed matter and atomic physics. Due to the complex interaction between projectiles with charge states $Q \gg 1$ and the multitude of target electrons involved in the neutralization process, a complete picture for electron capture, emission, and the formation of material defects remains challenging and has only been attempted for a few specific material systems, i.e., bulk metals [1] and bulk ionic crystals [2,3]. For these cases, the classical over-the-barrier (COB) model gives quantitative predictions that are in good agreement with electron emission statistics [4,5], x-ray spectra [6], and ion image acceleration measurements [7,8]. The foundation of the COB model is that the first electron transfer from target to ion occurs in a classically allowed region and populates a high n (principal quantum number) state in the ion. For HCIs approaching metal surfaces, filled levels in the metal become resonant with the high n states while the HCI is still a few nanometers from the surface. Consequently, initial charge transfer takes place predominantly via fast transitions over the top of the strongly perturbed vacuum potential barrier between the HCI and the surface. Once captured by the projectile, these electrons relax to inner-shell vacancies through the emission of Auger electrons and photons. The critical distance (R_c) for the onset of charge transfer can be well approximated using classical potentials [1] due to the "point-charge"-like nature of the ion at a relatively far distance from the target electrons. R_c and ion velocity (v_p) set a characteristic time scale ($\tau \approx R_c/v_p$) for above-surface electronic processes before ion impact.

Within the COB model, the basic material properties that govern the onset of above-surface neutralization and determine R_c are electron binding energy in the solid (work function) W, energy band gap E_G, and permittivity ϵ. The addition of a thin dielectric film on a metal surface introduces new W, E_G, and ϵ for the surface layers without modifying the bulk. Thus, experimentally, the deposition of a thin film provides a method for changing the electronic structure of the surface and testing the role of surface-versus-bulk material properties during HCI neutralization. This approach was used in a measurement of the above-surface emission of Auger electrons as a function of LiF film coverage on Au(111) up to 1 (monolayer) ML and served to decouple the role of target binding energy and band gap in K-shell filling for that system [9,10]. Those authors remark that even for a single monolayer of LiF coverage, the high binding energy of the LiF results in a suppression of the K-shell filling, suggesting that for LiF/Au(111), the target surface takes on the characteristics of the thin film rather than the bulk material.

In some cases, however, dielectric thin film covered targets retain the seemingly metallic character of the underlying bulk substrate. Recent results on HCI interactions with thin C_{60} films deposited on Au(111) show electron emission yields *increasing* as a function of the C_{60} film thickness [11]. This suggests that the increasing film thickness may enhance rather than suppress the efficiency of Auger relaxation relative to a clean metal surface, even after the deposition of ≈5 ML of dielectric material.

The seemingly contradictory results of LiF and C_{60} films on Au(111) motivate our application of the COB model to studying electron capture by HCIs above metal surfaces covered with thin dielectric films. Additionally, our recent charge dependent stopping power measurements [12] motivate a study of charge transfer above thin films. Until now, above-surface charge exchange for HCIs interacting with thin films has not been treated systematically with the COB model. In this article, we describe the application of the COB model to the initial charge exchange between HCIs and target electrons in solids covered with thin films. We develop a simple physical model that describes the crossover from the thin film to bulk target regimes as a function of the film's electronic properties and thickness. Adding a thin film to a bulk surface leads to

*Present address: COMP Centre of Excellence, Department of Applied Physics, Aalto University, P.O. Box 13500, 00076 Aalto, Finland; russell.lake@aalto.fi

new boundary conditions when constructing the electronic potential energy landscape and modifies the critical distance at which electrons can be captured by the ion. For the case of a metal surface covered with a thin dielectric film, we calculate ion capture distances and compare these results with bulk metal and dielectric targets. New studies of highly charged ion interactions with thin films will require this type of predictive model to gain insight into the role of bulk versus surface electrons during neutralization.

In this work, we find three distinct regimes for the onset of charge transfer as a function of the key parameters: thin film thickness, permittivity, binding energies, and dielectric band gap. These regimes are as follows: "vacuum limited" capture of electrons from the bulk metal (regime i), "film limited" capture of electrons from the bulk metal (regime ii), and capture of electrons from the thin dielectric film (regime iii). These three regimes bridge the classical over-the-barrier model for bulk metals and bulk dielectrics as the thickness of a dielectric film on a metal substrate increases.

The article is organized as follows. First, we introduce in Sec. II the basic framework and assumptions of the existing COB picture for electron capture by HCIs above bulk metal and insulator targets. Then, using the framework from Sec. II, we describe in Sec. III how the potential of an "active electron" in the first stage of above-surface neutralization is modified by the presence of a thin dielectric film at the surface. Also in Sec. III, we derive thickness dependent critical distances starting with parameters for ultrathin C_{60} films on Au(111), and the dependence of critical distances on film permittivity, band gap, and metal work function are discussed. In Sec. IV, we discuss comparisons between the model and three experimental systems: C_{60}/Au(111), LiF/Au(111), and Al_2O_3/Co. Finally, the results are summarized in Sec. IV D and Sec. V.

This article presents the revised version of a previously published model [13]. The main improvement in the model presented here is in the calculation of the ion's image potential as well as a more thorough discussion and interpretation of the dependences on charge state and target parameters. Here, we solve Poisson's equation exactly for the metal-dielectric-vacuum system, matching the boundary conditions at both the metal and dielectric surfaces. The previously published version did not include the electric field boundary constraint at the dielectric-vacuum interface. As will be shown below, both versions of the model demonstrate the same qualitative behavior when calculating electron capture distances. However, some numerical results change when discussing the Al_2O_3/Co system.

Our approach is not to compete with state-of-the-art theory or give an exact treatment. Rather, we provide a simple physical model that will apply generally to a wide variety of targets consisting of thin dielectric films on surfaces. The starting place for this study is the success of continuous band models used in device and solid-state physics [14,15]. When an HCI approaches a thin-film-covered metal target at normal incidence, the electric field applied in the direction connecting the ion and its image has the same z-dependent functionality as in a multilayer metal-insulator heterostructure. This similarity naturally leads to the "band bending" physics described in Sec. III.

II. BULK TARGETS

Since the work here is an extension of the COB modeling for bulk materials [1,16,17], we begin with a brief summary for the case of an HCI with initial charge state Q, at a distance R outside of a bulk surface. The potential energy V for an "active electron" in the region between the surface and the HCI is composed of three contributions: attraction between the electron and the ion (V_I), attraction between the electron and its own image (V_e'), and repulsion between the electron and the HCI's self-image in the target (V_I'):

$$V(z) = V_I(\mathbf{r},\mathbf{R}) + V_e'(z) + V_I'(\mathbf{r},\mathbf{R}). \tag{1}$$

The origin is set at the surface of the bulk where $\mathbf{r}$ and $\mathbf{R} = R\hat{z}$ are the position vectors for the electron and the ion, respectively. The target's electric permittivity ϵ modifies the image terms by a dielectric function $\beta = (\epsilon - 1)/(\epsilon + 1)$ (in atomic units):

$$V_I(\mathbf{r},\mathbf{R}) = -\frac{Qe}{|\mathbf{r} - R\hat{z}|}, \tag{2}$$

$$V_I'(\mathbf{r},\mathbf{R}) = \frac{\beta Qe}{|\mathbf{r} + R\hat{z}|}, \tag{3}$$

$$V_e'(z) = -\frac{\beta e^2}{4z}. \tag{4}$$

The distance R_c for COB capture of electrons from the target occurs where the maximum $V(z)$ between the HCI and the target drops below the highest occupied state in the target. From Eqs. (2)–(4), this critical distance is [16]

$$R_c \approx \frac{\sqrt{2Q\epsilon(\epsilon - 1)}}{W(\epsilon + 1)} + \frac{\epsilon - 1}{4W(\epsilon + 1)\epsilon}. \tag{5}$$

R_c has a square-root power-law dependence on the charge state, and inverse dependence on W. In the ideal metal case ($\beta \to 1$), the critical distance reduces to $R_c \approx \sqrt{2Q}/W$.

Equation (5) is applicable to metals and narrow band gap semiconductors [16] where the capture distance is greater than the dynamic screening length λ_d of the target electrons (e.g., $\lambda_D = v_f/\omega_s = 0.1$ nm for Au, where v_f and ω_s are the Fermi velocity and surface-plasma frequency, respectively) [17]. For ionic crystals, the expression in Eq. (5) breaks down as interactions between an electron in transit and discrete charges in the target (residual vacancies, ionic cores) increase in strength at close capture distances [2,3]. Equation (5) also differs from the general expression derived in Ref. [18], which includes the direct Coulomb interaction with the residual vacancy.

The question of correctness of the static versus optical dielectric functions for HCI-surface interactions (both with normal and grazing impact trajectories) has been addressed in the literature, in particular for LiF [2]. Here the authors show that neither the static nor optical permittivity perfectly models the dielectric response at finite velocities and that an exact calculation of the frequency-dependent dielectric function yields an intermediate value between these optical and static limits at normal incidence. For values greater than a characteristic time-scale parameter $(z + R)/v > 400$ a.u., the exact permittivity differs from the static limit by less than 50%.

For generality, we use the static permittivity limit as an input parameter of the model for the different materials discussed. This gives an upper bound for the dielectric screening and allows comparison between different systems. To account for time-dependent effects, ϵ and β can be treated with exact frequency (ω) dependent dielectric functions $\epsilon(\omega)$ and $\beta(\omega)$ [2].

III. DIELECTRIC THIN FILMS ON METALS

In this section, we modify the COB model result by adding a thin dielectric film on top of the metal, derive the modified distance (R_c'), and explore the dependence of R_c' on the important materials parameters. In comparison to the clean metal case, the presence of a dielectric thin film adds a new (metal-dielectric) interface and introduces a new boundary condition. The potential energy profile is constructed as shown in the point-charge schematic in Fig. 1(a). Both the ion and active electron induce dielectric responses within the target in Fig. 1(a). Matching the boundary conditions at both the metal-dielectric and dielectric-vacuum interfaces is accomplished using an infinite series of image charges with diminishing weights [19]. These series are represented by Q', e', and e'' in Fig. 1(a).

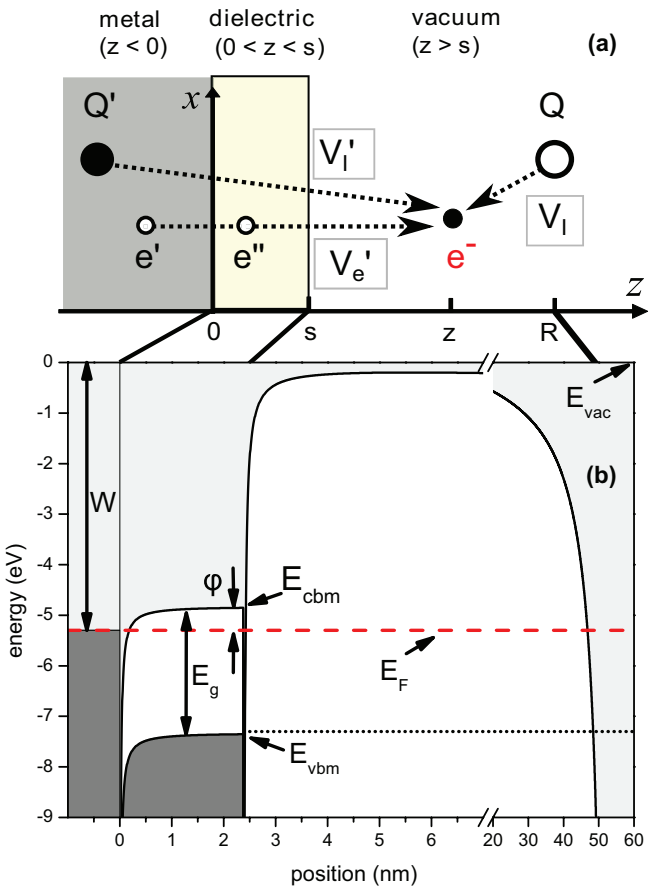

FIG. 1. (Color online) (a) Point charges are shown to represent the electron potential energy terms: HCI interaction (V_I), self-image (V_e'), and ion-image (V_I') terms. (b) Potential energy profile for an electron along z is shown when the ion is far (>50 nm) from the metal surface using parameters for a C_{60} film on an Au(111) substrate: $s = 2.4$ nm, $\epsilon = 4$, $E_g = 2.5$ eV, $W = 5.3$ eV, $\phi = 0.5$ eV, and $Q = 24$.

In Fig. 1(b), the potential energy for an active electron is plotted along the surface normal coordinate z for an ion position that is far from the surface ($R > 50$ nm). The potential energy is the sum of terms representing V_e', V_I, and V_I' depicted in Fig. 1(a). These potential energy terms are modified with respect to Eqs. (2)–(4) due to the new boundary conditions introduced by the presence of the thin film. In Fig. 1(b), the potential has a $-Q/|z - R|$ dependence in the vicinity of the ion. Near the surface, the image forces influence the shape of the potential. Image planes are formed at surfaces of both the metal and dielectric regions as described within the dielectric continuum model [20–24], which is discussed in context in Sec. III C.

A. Ion potential (V_I, V_I') and boundary conditions

We first consider the terms due to the ion and its dielectric response in the target (the electron's self-image term is discussed in Sec. III C). The general approach is to modify Eqs. (3) and (4) to account for the presence of a thin dielectric film. Obtaining the modified potential landscape requires a solution to Poisson's equation matching the following general boundary conditions [19,25]:

$$V = 0 \quad \text{at the metal surface,} \tag{6}$$

$$\Delta E_{||} = 0 \text{ and } \Delta D_{\perp} = 0 \quad \text{at the thin film surface.} \tag{7}$$

As in the clean metal case, the electron potential energy vanishes at the surface of the metal [Eq. (6)]. $\Delta E_{||}$ and $\Delta D_{\perp}$ are the differences in the electric field parallel to the surface and electric displacement normal to the surface at the interfaces. Solutions to Poisson's equation that match the boundary conditions in Eqs. (6) and (7) for metal-insulator-vacuum systems can be obtained using integral representations in cylindrical coordinates. The result is that the combined terms $V_I(\mathbf{r},\mathbf{R})$ and $V_I'(\mathbf{r},\mathbf{R})$ from Eq. (1) are replaced by the potentials matching the boundary conditions in Eqs. (6) and (7) and which are solved explicitly in Refs. [26,27], which we will call $V_{\mathrm{HCI}}(z)$.

The slope of the ion's potential in the film (electric field) decreases with increasing permittivity ϵ. For $\epsilon = 1$, the dielectric region has the same permittivity as the vacuum region, and there is no change to the slope of the potential within the film compared to the vacuum. As a check, we can consider when $\epsilon \to \infty$ and the potential energy in the film looks like that of an ideal conductor. Indeed, when $\epsilon = \infty$, the potential energy is the same as if the metal surface is just extended into the vacuum by the thickness of the film s. In this limit, the film perfectly screens the external charge Q and the potential vanishes at $z = s$ satisfying Eq. (6). The film permittivity governs the potential barrier height for electrons in the metal in the region $0 < z < s$ by modifying the electric field strength due to the charge Q.

B. Energy levels in the solids

The thin dielectric film is represented in the model by four important parameters: the film thickness s, the film's electric permittivity ϵ, the bottom of the conduction band E_{cbm}, and

the top of the valence band E_{vbm}. For the purposes of this model, we assume that above the film's conduction band minimum, the film is composed of a continuum of allowed states that permit the transport of electrons easily from the metal. Similarly, below the valence band, we assume the levels are filled with a reservoir of electrons that are available to be captured by the incoming HCI if the vacuum barrier should fall low enough to permit charge transfer. However, since the thin film has no free charge, as the ion approaches, its strong electric field will bend the bands of the insulator and pull down both the conduction and valence bands on the vacuum side, while the metal side will remain unperturbed. To account for this effect, the conduction band $V_{cbm}(z)$ and valence band $V_{vbm}(z)$ are referenced to the perturbed "vacuum" energy, i.e., they are less than the value of $V_{\mathrm{HCI}}(z)$ by the value E_{cbm} and E_{vbm}, respectively. This maintains a constant gap energy E_{gap} for all values of z through the dielectric film. This effect can be seen clearly in later figures where the ion is close enough to the surface to strongly perturb the film's energy levels.

Similarly, the metal (in the region $z < 0$) is parametrized as a continuum of filled states up to the Fermi energy E_F. The vacuum work function W is the difference between the Fermi energy (E_F) and the vacuum level (E_{vac}).

C. Electron self-image

Since we are interested in the potential experienced by a real charge (as opposed to a virtual test charge) transferring to the HCIs, we must consider the effect of the electron's self-image. The self-image is described using an electrostatic model developed by Cole to describe electrons trapped in image potential states at the surfaces of dielectric films on metals [24] using classical electrostatics for a thin homogeneous dielectric slab lying on a metal substrate. This approach is called the dielectric continuum model (DCM) and appears in various forms in the literature [20–23].

Here we use the DCM to describe an electron's self-image (V_e') in Fig. 1(a). Due to the discontinuity in ϵ across the dielectric-vacuum interface, the electron's image potential is defined piecewise between the vacuum region outside the film and inside the film. For the vacuum region outside the film, the image potential is

$$V_{\mathrm{out}}(z,s) = \frac{-\beta e^2}{4(z-s)} + \frac{(1-\beta^2)e^2}{4\beta}\sum_{n=1}^{\infty}\frac{(-\beta)^n}{z-s+ns}. \quad (8)$$

The first term is the image potential outside a semi-infinite dielectric, and the sum expresses the series of corrections due to the presence of the metal substrate, and the finite thickness of the film.

Inside the dielectric, the image potential is screened by the dielectric media as ϵ^{-1}. Additionally, within the film, the reference energy becomes the conduction band V_{cbm} instead of the vacuum level:

$$V_{\mathrm{in}} = E_{cbm} - \frac{e^2}{4\epsilon z}. \quad (9)$$

Equation (9) differs from the expression for V_{in} given in Ref. [22] which leads to a positive singularity at the dielectric-vacuum interface. Instead, the image potential shown above tends toward the solid-state value of E_{cbm} at the surface of the dielectric film [20]. The behavior of the self-image term treated with the DCM is shown in Fig. 1(b). The image forces pull down the bands in the dielectric film in close proximity to the metal surface. Figure 1(b) also displays an energy gap $\phi = \max(V_{cbm}) - E_F$ within the film whose height is determined by the relative alignment of the Fermi energy in the metal and conduction band minimum of the dielectric. ϕ is the potential barrier between electrons in the metal and the vacuum in the region $0 < z < s$, and will depend on R, ϵ, Q, and s.

D. Evaluating the critical distance R_c'

Starting with the potential diagram in Fig. 1(b), we pose the question of whether electrons in the dielectric or metal transit first, as the ion moves toward the surface. The metal has filled levels up to E_F, but is buried underneath the dielectric film. On the other hand, the surface of the dielectric film is exposed to the vacuum but contains more tightly bound electrons than in the metal [$V_{vbm}(s) \ll E_F$].

Figure 1(b) displays the two relevant energy barriers between metal target electrons and the ion. First, the barrier of approximate height ϕ and width s defines an energy barrier within the dielectric material. This barrier is defined by the portion of the dielectric's band gap that extends above E_F. Second, a vacuum barrier with approximate height W and width $(R - s)$ exists in the region outside the dielectric film ($z > s$).

As the ion approaches the surface, its electric field decreases the heights of both of the barriers until they fall below E_F and transport from electrons in the metal becomes classically allowed. Alternatively, electrons from the valence band in the dielectric film can be captured by the ion when the height of the vacuum barrier $\max[V(z > s)]$ falls below $V_{vbm}(s)$.

The ion's position outside the target when either classical transport condition is met is the critical distance R_c' for the onset of charge transfer. For very thick films, the target behaves similar to a bulk insulator, and the first electron will be captured from the valence band of the dielectric thin film.

The critical distance for a given charge state, therefore, will depend on the initial width and height of the barriers in the film and vacuum regions (for electrons in either the film or metal). The physical parameters that set the initial height and width of these barriers are the film thickness s, film permittivity ϵ, and relative alignment of E_{vbm}, E_{cbm}, and E_F with respect to the vacuum level. As shown below, these parameters will also determine whether the first electron will be captured from the metal or the dielectric thin film.

Figures 2(a)–2(c) shows the evolution of the barrier heights in the vacuum and in the dielectric regions as the ion ($Q = 24$) approaches the surface. The metal's Fermi level is plotted as a horizontal line in each of the plots ($E_F = -5.3$ eV). The energy of the valence-band electrons $V_{vbm}(s)$ is plotted as a dotted line from where it is bent down by the impinging ion's electric field. The energy gap in the dielectric ($E_g = 2.5$ eV) and the nonconducting region of the vacuum are denoted as white space. The continuum of filled states in the metal and dielectric valence bands are shown in dark gray and the unoccupied states in the conduction bands are filled in light

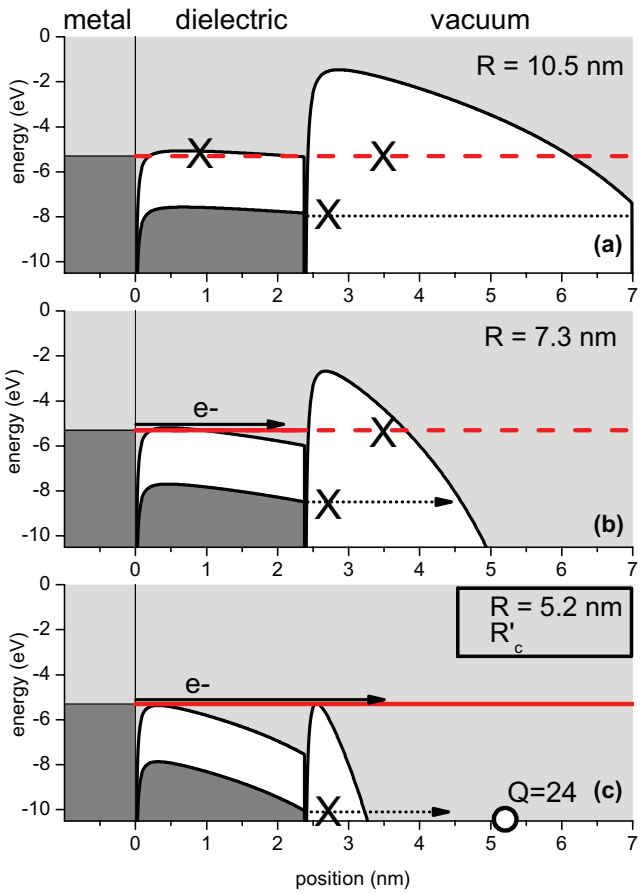

FIG. 2. (Color online) Potential profiles for an ion ($Q = 24$) at distances (a) $R = 10.5$ nm, (b) $R = 7.3$ nm, and (c) $R = 5.2$ nm away from the metal surface. Film parameters are $s = 2.4$ nm, $\epsilon = 4$, $E_g = 2.5$ eV, initial $\phi = 0.5$ eV, and $E_F = -5.3$ eV [dashed line in (a), (b) and solid line in (c)]. The valence-band energy $V_{vbm}(s)$ is plotted as a dotted line. Critical distance $R_c' = 5.2$ nm is shown in (c).

gray. Figures 2(a)–2(c) plot the potential profile in the vacuum and dielectric regions as the ion approaches the target and reaches distances from the metal surface of $R = 10.5$ nm, $R = 7.3$ nm, and $R = 5.2$ nm. Parameters are chosen to represent a $s = 2.4$-nm-thick C_{60} film deposited on Au(111).

Ultrathin C_{60} films have a highest occupied molecular orbital (HOMO) to lowest unoccupied molecular orbital (LUMO) gap of approximately $E_g = 2.5$ eV and the Fermi energy of Au(111) substrate lies within the band gap ($E_F = -5.3$ eV) of the dielectric film, making $\phi = 0.5$ eV [28]. The position of the valence-band maximum in the absence of an external field is $E_{vbm} = -7.3$ eV. Electric permittivity of the film is taken to be $\epsilon = 4$ [29,30]. The energy levels were taken from Refs. [11,28].

As the ion approaches the surface, a maximum in the potential energy profile along z develops in the vacuum ($s < z < R$) due to competition between the ion's electric field and the electron's self-image attraction toward the surface of the film ($z = s$). This behavior is qualitatively similar to the saddle point in front of a clean metal target. However, in Fig. 2, a second potential maximum develops within the dielectric material ($0 < z < s$) as the ion pulls down V_{cbm} and due to the electron's image attraction toward $z = 0$. In this case, we demonstrate that classical transport will be allowed first from the metal.

Following the ion's approach in more detail beginning at an ion distance of $R = 10.5$ nm in Fig. 2(a), the ion's electric field decreases the height of the vacuum barrier and bends the bands in the dielectric film to decrease the height of ϕ. At this ion position, metal electrons at E_F are blocked by the energy barriers in the film and in the vacuum (depicted as the white area in the film above E_F). Electrons at $V_{vbm}(s)$ in the dielectric are also blocked by the vacuum barrier and so no classical transport is allowed.

As the ion approaches to $R = 7.3$ nm in Fig. 2(b), the film's barrier has dropped to approximately the energy E_F so that $\phi = 0$. Here, only the vacuum barrier prohibits classical transport from electrons in the metal into the vacuum, and metal electrons could occupy available states in the conduction band near the dielectric-vacuum interface. The film's electrons at $V_{vbm}(s)$ are blocked by the vacuum barrier, so there is still no classical transport allowed.

As the ion arrives at $R = 5.2$ nm in Fig. 2(c), the barriers in both the vacuum and dielectric have fallen below E_F. Electrons at energy $V_{vbm}(s)$ in the valence band of the dielectric cannot escape due to a large potential barrier remaining in the vacuum. Thus, the first electron to be captured by the ion originates from the metal. This distance is R_c', i.e., the critical distance for electron capture by HCIs outside a metal covered with a dielectric thin film.

Comparing R_c' to the predicted critical distance for a clean Au target from Eq. (5) in the limit ($\beta \to 1$), we find that $R_c' = 5.2$ nm is greater than the result expected for a clean metal of $R_c = 1.9$ nm. For these parameters, the thin dielectric film enhances the critical distance by more than a factor of 2 compared to clean Au. In the case when an ion approaches a bare metal surface, the final vacuum barrier limiting charge transfer is located very close to the surface, since the free charge in the metal screens the electric field and the electron potential remains close to the vacuum potential at the surface. By introducing a film on the metal surface, the initial energy barrier is much lower, and therefore can be pulled down by the ion's electric field more easily, making charge transfer possible when the ion is much farther from the surface. The net effect is that the insulating film acts to help "impedance match" the metal states to the continuum above the surface.

In the next sections, we investigate the experimental parameters that lead to the enhancement of critical distance due to the deposition of a thin film ($R_c' > R_c$). Although this case demonstrated an enhancement, some thin dielectric films can suppress, or completely block, classical transport from the metal.

E. Three regimes of electron capture

In the previous section, we saw that a total of three different electron reservoir and energy barrier combinations exist. Here we show that each of these combinations results in a different electron capture regime. For a carefully selected set of parameters (in this case representing a 3.4-nm thick C_{60}/Au(111) system [11]), simply changing the charge state can illustrate each of the three regimes (Fig. 3). These regimes are vacuum limited electron capture from the metal (regime i),

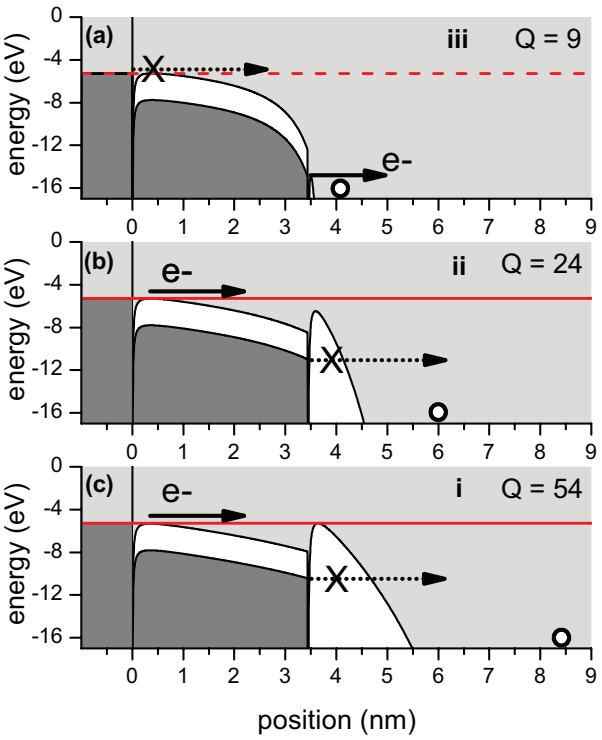

FIG. 3. (Color online) For 3.4 nm of C_{60} on Au(111), we show electron potential energy plots at R_c' for charge states $Q = 9,24,54$ in regimes iii, ii, and i, respectively.

film limited electron capture from the metal (regime ii), and electron capture from $V_{vbm}(s)$ in the dielectric film (regime iii), shown in Figs. 3(a)–3(c), respectively.

1. *Regime i: Vacuum limited capture from the metal*

Charge transfer from the metal can be limited either by the potential barrier ϕ or by the vacuum potential barrier.

Examples of potential energy plots for the vacuum limited regime i are shown in both Figs. 2(c) and 3(c). In both of these cases, as the ion approaches the surface, the barrier (ϕ) drops below E_F before the barrier in the vacuum drops below E_F. Therefore, in regime i, the classical electron capture distance is determined by the vacuum barrier.

This regime occurs for higher charge states where the longer spatial influence of the ion's potential can reduce ϕ fast enough with respect to W that classical transport is permitted through the dielectric. Although it is somewhat difficult to see in Fig. 3(c), $\phi < 0$ while E_F is equal to the barrier in the vacuum.

2. *Regime ii: Thin film limited capture from the metal*

For thicker films, higher initial ϕ barriers, greater film permittivity, or lower HCI charge states [as shown in Fig. 3(b)], the capture of an electron from the metal can be limited by ϕ instead of the vacuum barrier. In this film limited regime, the vacuum barrier drops below E_F while $\phi > 0$, as shown in Fig. 3(b).

This means that for ion distances slightly greater than R_c', the potential maximum in the vacuum has already fallen below E_F. Immediately before the charge transfer channel opens, the only barrier limiting capture is ϕ. Due to the lower charge state, the ion has a shorter spatial influence and more weakly reduces ϕ than in regime i so that ϕ can still remain even when the vacuum barrier is well below E_F.

3. *Regime iii: Capture from the dielectric*

For $Q = 9$ in Fig. 3(a), where the first captured electron originates from the valence band of the dielectric at a distance $R_c' = 4.0$ nm from the metal. The influence of the ion on the energy barrier ϕ is sufficiently weak that electrons in the metal are blocked, while transport from $V_{cbm}(s)$ is classically allowed. At this point, the target appears to the ion like a bulk dielectric material. The metal substrate is shielded by the dielectric film and the metal work function plays no role in determining the critical distance. In this regime, the COB model for bulk insulators becomes applicable [2] and the critical distance is described by Eq. (5), i.e., E_{vbm} and ϵ uniquely determine the onset of classically allowed charge transfer.

F. Film permittivity dependence

One of the most important material parameters to influence ϕ is ϵ. In Fig. 4, we vary ϵ while keeping the ion $Q = 24$ at $R = 6$ nm to illustrate the role of ϵ. For reference, the unperturbed electron potential is plotted as the black solid line. The valence bands within the dielectric have been removed from the plot for clarity. Inside the film, the ion bends the conduction band, lowering the barrier ϕ from its initial height. The magnitude of the band bending depends inversely on the ϵ of the film material. In the vacuum region outside the film, the potential maximum also varies inversely with ϵ due to the boundary condition at the film-vacuum interface. In this way, ϵ strongly influences the barrier heights in both the thin film and vacuum regions.

The solid orange line in Fig. 4 plots the potential using the same permittivity and gap parameters as those plotted in Fig. 2(b), except that in Fig. 4, the film thickness has been increased to $s = 4$ nm. This position is the critical capture distance $R = R_c'$ and the ion can classically capture an electron from the metal.

The blue dotted line in Fig. 4 shows the effect of increasing ϵ to 10. This weakens the electric field within the film causing less band bending and increases ϕ. Consequently, the position $R = 6$ nm is greater than the critical distance. On the other hand, the green line shows the potential for $\epsilon = 3$, which increases the electric field strength and reduces the barrier heights inside the film and in the vacuum. At $R = 6$ nm, an electron in the metal could have easily transferred at $R > 6$ nm. In general, decreasing ϵ increases the critical capture distance. For a constant set of target material properties and film thickness in Fig. 4, we see qualitatively from the potential maxima that $R_c'(\epsilon = 10) < R_c'(\epsilon = 4) < R_c'(\epsilon = 3)$.

To show more explicitly how the critical distance R_c' depends on the film permittivity ϵ, Fig. 4(b) plots $R_c'(\epsilon)$ for film thickness $s = 4$ nm and charge $Q = 24$ over the range $\epsilon = 1$ to $\epsilon = 10$. As expected, the general trend is that R_c' decreases as ϵ increases from 1 to 10. In the regions of the plot labeled i and ii, the first captured electron originates from the metal. As permittivity increases, the electric field that is needed to pull down ϕ also increases. This means that

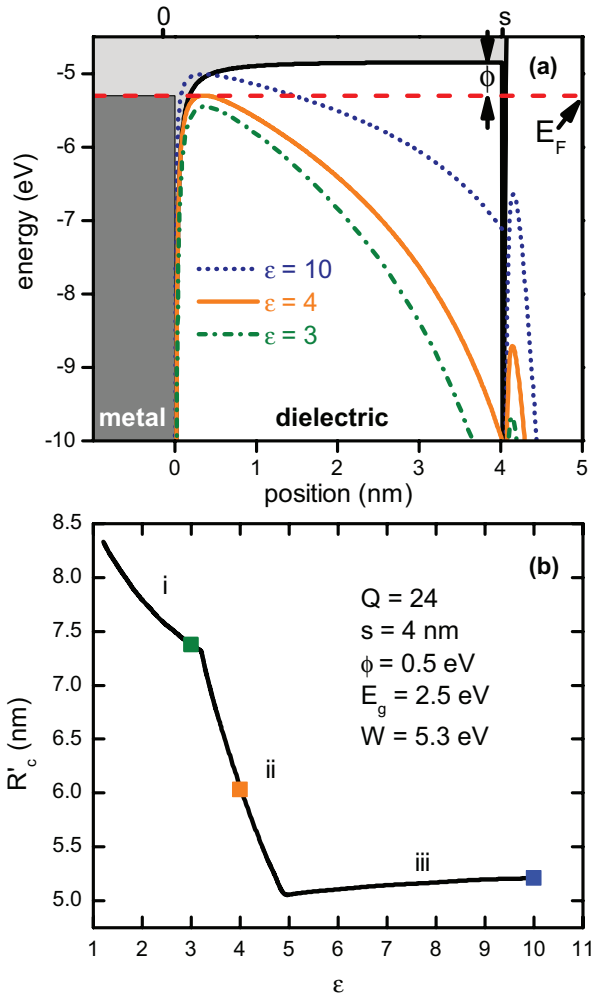

FIG. 4. (Color online) (a) Dependence of the potential barrier maxima on film permittivity. The solid black line plots the unperturbed barriers in the vacuum ($z > s$) and film ($0 < z < s$) for reference. The other lines plot $R = 6$ nm with $\epsilon = 10$ (dotted line), $\epsilon = 4$ (dashed line), and $\epsilon = 3$ (solid green line). (b) Critical distance as a function of film permittivity with capture regimes i, ii, and iii indicated. Parameter values in (b) apply to both panels.

an ion of a given charge state must be in closer proximity to the target before it can exert the electric field required to reduce ϕ. In Fig. 4, this is the reason that R_c' decreases with increasing ϵ. In the region of the plot in Fig. 4(b) labeled iii, the first captured electron comes from the filled states in the dielectric film. These are the same regimes described in Sec. III E and, like with Q, the parameter ϵ can vary the charge transfer regime through all three types. This serves to emphasize the importance of accurate knowledge of ϵ when modeling experimental systems.

G. Work function dependence

To further illustrate the dependence of the three regimes on materials parameters, in Fig. 5 we show $R_c'(s)$ for a range of metal work functions between 4 eV and 7 eV, leaving the parameters ϕ and ϵ unchanged. In order to keep ϕ constant, E_{cbm} increases with the metal work function. For a single material system when s is the only parameter varying, we

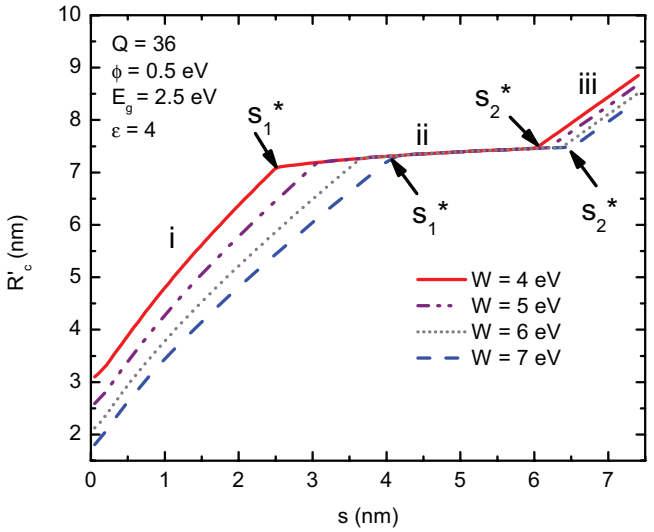

FIG. 5. (Color online) The critical distance as a function of film thickness for different metal work functions between $W = 4$ eV and 7 eV. Since ϕ is kept constant, $R_c'(s)$ is independent of W in regime ii .

define the critical thicknesses s_1^* and s_2^* to denote the value of s where the charge transfer regime changes from i to ii, and ii to iii, respectively. Comparing $R_c'(s)$ versus s for different work functions while leaving all other parameters constant provides a clear demonstration that only ϕ limits transport from the metal in regime ii, where $s_1^* < s < s_2^*$ and the critical distance is independent of the metal work function. ϕ, ϵ, and Q determine $R_c'(s)$ in regime ii. For film thicknesses below s_1^*, the vertical intercept of R_c' has a relatively strong $(1/W)$ dependence on work function. Additionally, s_1^* increases by approximately 2 nm as W increases from 4 eV to 7 eV.

On the upper end, s_2^* has a weak dependence on work function, i.e., it increases by only a few angstroms as W increases from 4 eV to 7 eV.

H. Critical distance as a function of film thickness

As was also seen in Fig. 5, R_c' depends on film thickness, progressing from vacuum limited to film limited capture from the metal and, finally, capture from the insulator as s increases. When $s = 0$, no barrier in the film exists, and as s is increased, the primary effect is that the vacuum barrier is pushed further from the surface. The further the vacuum barrier is from the surface, the less effective the metal is at holding up the vacuum potential and the more effective the ion is at pulling it down. However, the maxima in ϕ replaces the vacuum barrier close to the surface, and as s increases, the vacuum barrier is pulled down much faster relative to ϕ. The value $s = s_1^*$ is the thickness and R where both the vacuum barrier and ϕ fall to E_F at the same time. Q, ϵ, and s all affect the "lever arm" for how strongly ϕ is perturbed relative to the vacuum barrier, and therefore the value of s_1^*. For larger values of s, R_c' is then determined by ϕ.

The R_c' dependence of this lever arm on Q and ϵ is shown in Fig. 6, where the slope of R_c' and values of s_1^* and s_2^* are all affected. In both panels of Fig. 6, we use the band gap, ϕ barrier, and metal work function values for C_{60} on Au(111). The solid orange line in both Figs. 6(a) and 6(b) plots critical distance as a

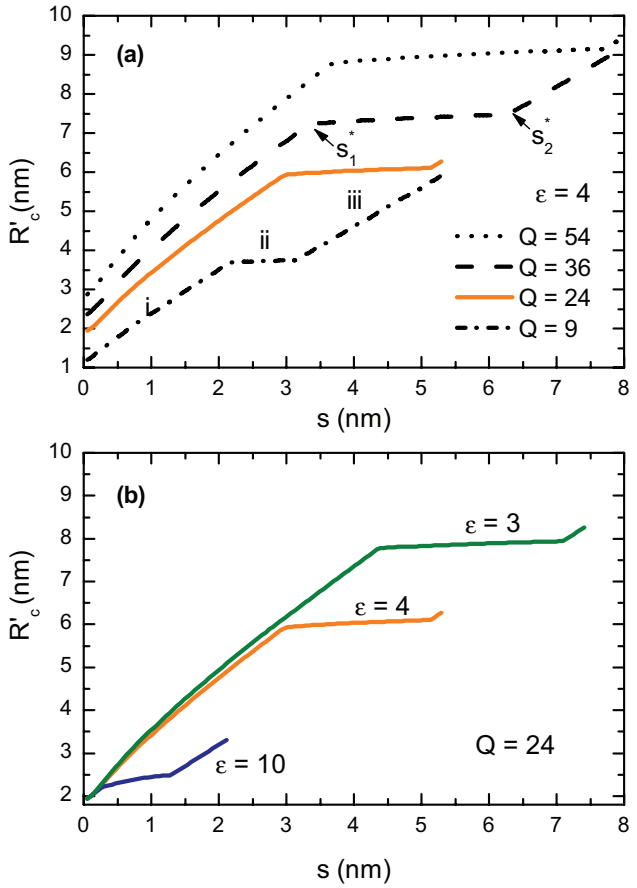

FIG. 6. (Color online) (a) $R_c'(s)$ for charge states $Q = 9$, 24, 36, and 54. The first captured electron comes from the metal substrate in i and ii, and from the valence band of the dielectric film in iii. (b) $R_c'(s)$ for $\epsilon = 3$, 4, and 10 at $Q = 24$. Parameters in Fig. 4(b) apply to both panels, except as noted.

function of film thickness for $\epsilon = 4$ at $Q = 24$, for comparison with previous figures and experiment (discussed later).

The value of R_c' at $s = 0$ in Fig. 6 is the clean metal limit where no film is deposited [Eq. (5) with $\beta \to 1$]. Increasing the charge state increases the capture distance at $s = 0$ as $\sqrt{Q}$. As s increases, R_c' for each charge state in Fig. 6(a) follows similar qualitative behavior, and demonstrates the distinct regimes labeled i, ii, and iii. In regime i, R_c' grows almost linearly with a slope greater than 1 up to s_1^*, i.e., the capture distance is increasing faster than the film thickness and the film is enhancing charge transfer.

In regime ii ($s_1^* < s < s_2^*$), the slope of R_c' is almost flat compared to region i. Regime ii corresponds to film limited capture of metal electrons. For a fixed set of parameters, the ion must approach to almost the same R regardless of s to pull down ϕ, which is held up by the metal states. As $s \to s_2^*$, R_c' is increasing little and the film surface is getting closer and closer to the ion. Consequently, the vacuum barrier preventing charge transfer from $V_{vbm}(s)$ is dropping quickly as s increases until charge in the dielectric is no longer bound. Once s reaches s_2^*, the charge transfer crosses to regime iii, where the first electron is captured directly from the valence band of the dielectric material. As s increases further, ϕ increases when the ion is at R_c' preventing any charge transfer from the metal. Functionally, $R_c'(s) = R_c'(s_2^*) + s$, since the charge is captured from the film and s no longer influences the capture distance from the dielectric (R_c' is the distance from the metal-dielectric interface.)

R_c' in regime iii is also the same value given by Eq. (5), i.e., the classical over-the-barrier model for bulk insulators is recovered [2].

Considering the electrostatics, the transition between vacuum limited (regime i) and film limited (regime ii) capture of an electron in the metal at s_1^* can be interpreted in the following way. For a constant ion position R, increasing the film thickness will *decrease* the distance between the ion and image plane at the surface of the film ($z = s$). The strength of the image attraction in V_{out} [Eq. (8)] scales approximately as $-1/z$ and asymptotes at $z = s$. This means that the magnitude of the image potential grows rapidly as the distance between the ion and the image plane ($z = s$) is decreased. The result is that increasing the film thickness will diminish the vacuum barrier maximum at greater R values. At the thicknesses greater than s_1^*, the film has been extended a sufficient amount such that V_{out} pulls the maximum of the barrier in the vacuum below E_F, before the barrier ϕ can be pulled below E_F by the ion's electric field.

The transition thickness s_2^* is a prediction for the film thickness at which there is equal probability of classical capture of an electron from either the metal or dielectric film. At thicknesses greater than s_2^*, electrons will be captured (over the vacuum barrier) from the valence band of the dielectric film, while electrons in the metal are blocked by the energy gap ϕ within the film. So for $Q = 24$ in Fig. 6, the dielectric will look like a bulk to the ion at a transition thickness of $s_2^* = 5.1$ nm.

It is also worth noting that at the film thickness of $s = 3.4$ nm in Fig. 6(a), the regime of R_c' will depend on the charge state of the ion. For example, $Q = 9$ is in regime iii, $Q = 24$ is in regime ii, and $Q = 54$ is in regime i. The potential profiles for each of these charge states is shown in Fig. 3.

Figure 6(b) is essentially the same as Fig. 6(a), except that the different traces are for different permittivity values. Comparing the case of $\epsilon = 3$ and 4, the physics of the charge transfer can be quite sensitive to ϵ. Further, for high ϵ values ($\epsilon > 10$), the s_1^* is smaller than a typical atomic unit cell. Physically, this means that for any film with a high permittivity, no vacuum limited regime for electron capture from the metal will exist. An experimental example of this behavior will be discussed in Sec. IV C for the case of Al_2O_3 film on Co.

Figure 7 presents a map of regimes i, ii, and iii as a function of film thickness and charge state for the target parameters given in Fig. 6(a). The dotted line is the transition thickness s_1^*, which separates vacuum limited electron capture from the metal in regime i from film limited electron capture from the metal in regime ii. This transition thickness s_1^* increases with increasing charge state according to the relationship $s_1^* \propto Q^{0.3}$.

The transition film thickness s_2^* is plotted as a function of charge state in Fig. 7 as a solid line. This line distinguishes film limited electron capture from the metal (regime ii) from electron capture from the valence band of the dielectric film (regime iii). This transition increases with increasing charge

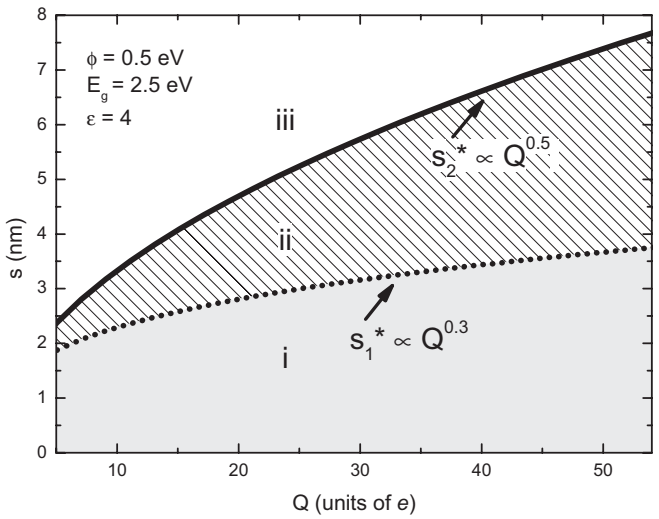

FIG. 7. Map of the regimes i, ii, and iii for film thickness and charge state with $W = 5.3$ eV, $E_g = 2.5$ eV, and $\phi = 0.5$ eV. The transition thicknesses s_1^* and s_2^* appear to follow power laws of $Q^{0.3}$ and $Q^{0.5}$, respectively (empirical).

state as $s_2^* \propto Q^{0.5}$, i.e., the same power dependence as the COB model.

All film thicknesses smaller than s_2^* lead to an enhancement of capture distance with respect to the clean metal for the film parameters in Figs. 6 and 7. When s reaches s_2^*, the dielectric can shield the metal electrons from ion capture and the COB model for insulators becomes a relevant description [2,3].

IV. COMPARISON WITH EXPERIMENT

A. C_{60}/Au(111): Electron emission yield

Critical distance may be correlated with an experimental observable such as electron emission yield, assuming that the total potential emission per incident ion is proportional to the above-surface interaction time ($\tau' = R_c'/v_p$). R_c' determines the onset of neutralization and may be proportional to the total yield of Auger electrons emitted above the surface before impact. The experiment in Ref. [11] reports measurements of electron emission yields for Xe^{24+} incident on C_{60} covered Au(111) at an incidence angle of 40° at 70 keV. Yield due to kinetic emission is expected to be negligible in the measurement. The data in Fig. 8 is taken directly from Ref. [11] where the relative secondary electron yield is plotted as a function of C_{60} film thickness Θ in monolayers (ML), and relative secondary electron yield is defined as

$$\gamma^{\mathrm{rel}}(\Theta) = \frac{\gamma^{C_{60}}(\Theta)}{\gamma^{\mathrm{Au}}(\Theta = 0)}, \tag{10}$$

where γ is the number of secondary electrons emitted per incident ion, and $\Theta = s/t_{\mathrm{ML}}$. The thickness of a C_{60} monolayer is in the range of $t_{\mathrm{ML}} \approx 0.7$ nm to 0.8 nm [11]. Also in Fig. 8, we plot the critical distance normalized by critical distance at $s = 0$ nm (R_c'/R_c) from 0 ML to 5.5 ML. The thickness of a single monolayer of C_{60} was taken to be $t_{\mathrm{ML}} = 0.75$ nm. The quantity (R_c'/R_c) is proportional to the relative increase in interaction time due to the thin film (τ'/τ). The charge state in both experiment and model is $Q = 24$.

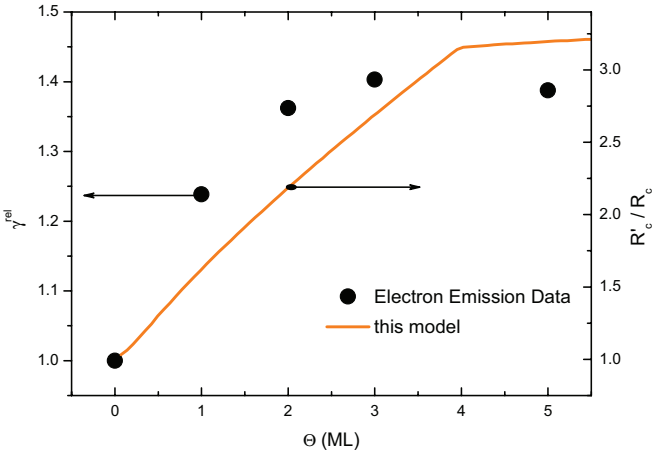

FIG. 8. (Color online) (a) Relative emission yield measurements for Xe^{24+} incident on C_{60} covered Au(111) taken from Ref. [11]. (b) Film thickness dependent critical distance (R_c') normalized by the critical distance for a clean metal. The horizontal axis in (b) is determined by $\Theta = s/t_{\mathrm{ML}}$, where $t_{\mathrm{ML}} = 0.75$ nm.

The knee in the calculated line in Fig. 8 corresponds to the transitions between regimes i and ii at $s_1^* = 3$ nm (4 ML). Comparing the data and model in Fig. 8, we make several observations. First, for the film thicknesses used in the experiment, the model predicts that the first captured electron originates from the metal and not the C_{60} film. All thicknesses shown are below the thickness $s_2^* = 5.1$ nm (6.8 ML) calculated for Xe^{24+}. Second, based on the model, we expect enhanced critical distances for thicknesses below $s_2^* = 5.1$ nm. The model for thin-film-enhanced critical distances follows the behavior of the increase in relative yield observed in the data.

One possible explanation for the good agreement is that enhanced capture distances lead to enhanced yields by increasing above-surface interaction time. Finally, the saturation in relative yield shown occurs at thicknesses ($s \approx 2$ nm or 2.7 ML) that are close to the calculated s_1^*. For $Q = 24$, the transition from the vacuum limited to the film limited regimes occurs at $s_1^* = 3$ nm (4 ML). It is plausible that the saturation in relative yield in the data occurs near s_1^* due to this transition.

B. LiF/Au(111)

HCI interactions with lithium fluoride has been the subject of many studies, including LiF thin films on Au(111). Lithium fluoride in bulk is an ionic crystal with a large band gap $E_g = 14$ eV and valence-band maximum ($E_{vbm} = 12$ eV). Consequently, in bulk, its conduction band exists in the positive continuum, above the vacuum level. In the formalism of our model, the presence of a large band gap means that electrons in the metal would be blocked by an initial barrier ϕ whose height exceeds the typical vacuum work function of a metal, i.e., there would never be a regime i since more energy is required to inject an electron into LiF than vacuum. This means that the film would immediately suppress electron emission compared to a bare metal surface.

We can compare this prediction with above-surface KLL Auger electron spectra taken during neutralization of O^{6+} and N^{7+} in Refs. [9,10]. These results imply a strong suppression of

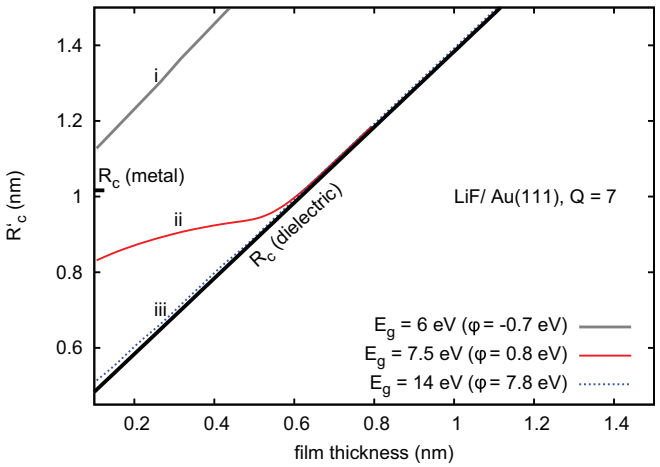

FIG. 9. (Color online) $R_c'(s)$ for $Q = 7$ outside LiF/Au(111). Electrons in the dielectric have fixed binding energy of 12 eV. With (bulk) band gap $E_g = 14$ eV, the first capture proceeds from the dielectric. A reduced band gap $E_g = 7.5$ eV leads to capture from the metal with suppressed R_c' below $s = 0.5$ nm. $E_g = 6$ eV facilitates capture compared to a clean metal due to $\phi < 0$ eV.

R_c' even after only 1 ML of LiF growth. The authors concluded that 1 ML of LiF is sufficient to effectively "shield" the Au substrate during the neutralization sequence. Thin LiF films cause a delay in the onset of first capture and decrease the rate of above-surface neutralization [9]. However, the large gap observed in bulk LiF develops [9,10] only after thicknesses of about five monolayers (1 ML ≈ 0.4 nm [31]). In contrast to the bulk band gap, LiF develops the high bulklike binding energy $W = E_{vbm} = 12$ eV even at submonolayer thicknesses. Thus, those authors argued that the large binding energy (and not the band gap) was the limiting factor in determining the onset of above-surface neutralization. In short, the binding energy of an electron in the thin dielectric film was held primarily responsible for the observed suppression in the above-surface component in the Auger spectra. This interpretation implies that the first captured electrons originate from the LiF film rather than the metal.

To analyze this scenario using the model presented here, we plot R_c' as a function of film thickness for a $Q = 7$ projectile outside the surface of LiF/Au(111) in Fig. 9. The LiF films are parametrized as having permittivity $\epsilon = 9$ and binding energy $E_{vbm} = 12$ eV. The solid lines in the plot represent the expected capture distances from Eq. (5) in the bulk metallic and bulk dielectric limits. To investigate the role of the band gap in the suppression of electron capture, we varied the band gap of the LiF films between the bulk value $E_g = 14$ eV and a reduced value of $E_g = 6$ eV. The results for $E_g = 14$ eV, $E_g = 7.5$ eV, and $E_g = 6$ eV are plotted in Fig. 9. In our model, we reference the barrier in the dielectric film to the Fermi energy of the metal as $\phi = E_{vbm} + E_g - E_F$. Therefore, the band gaps $E_g = 14$ eV, $E_g = 7.5$ eV, and $E_g = 6$ eV correspond to barrier heights in the dielectric of $\phi = 7.3$ eV, $\phi = 0.8$ eV, and $\phi = -0.7$ eV, respectively.

For the smallest band gap $E_g = 6$ eV, the barrier within the dielectric film vanishes ($\phi < 0$ eV), and the dielectric film's conduction band would fill up to E_F and facilitate the capture of electrons in the metal. Increasing the band gap to $E_g = 7.5$ eV, the model shows that capture of electrons from the metal behind the ultrathin LiF film is suppressed below $s < 0.5$ nm. The onset of capture is delayed for film thicknesses comparable to 1 ML of LiF, as seen in the experiment. Finally, for the full band gap $E_g = 14$ eV, we observe an even stronger suppression of R_c'. The first captured electrons come from the valence band of the LiF, and not the metal. This leads to decreased capture distances compared to a clean gold target (Fig. 9, short blue dashes). Consequently, the blue dashed line converges to the capture distance given in Eq. (5).

For comparison, the bulk dielectric and bulk metal limits for R_c' are shown as solid black lines in Fig. 9. These were obtained using Eq. (5) with permittivities of $\epsilon \to \infty$ for the metal and $\epsilon \to 9$ for the LiF film. The effective "work function" for the dielectric is its binding energy $W = E_{vbm}$. Again, the R_c' are plotted in Fig. 9 with respect to the surface of the metal at $z = 0$. This means that the distance between the ion and the metal surface at the position of capture grows linearly with s when the electron originates from the dielectric. Our modeling shows that a reduced band gap, $E_g > 7.0$ eV, can result in the suppression of electron emission. The presence of such a nonzero yet reduced band gap in ultrathin LiF film is supported by measurements [32,33]. On the other hand, LiF possesses the high binding energy ($E_b = 12$ eV) at submonolayer coverages.

For the case of a nonzero yet reduced band gap, above-surface neutralization would begin with over-the-barrier capture of an electron from the metal and not the LiF valence band at a thickness of $s = 1$ ML. The model predicts that the limiting factor determining the onset of neutralization (from capture of metal electrons) is then the height of the barrier ϕ, which is based on the relative alignment of E_F in the metal and E_{cbm} in the LiF film. This scenario involving initial capture of metal electrons is in apparent contrast to the one proposed in Refs. [9,10], where the binding energy of the LiF film was held primarily responsible for the suppression of R_c' (implying that the first captured electrons originate from the ultrathin LiF film). However, capture of electrons from the metal behind the LiF film predicted by our model remains consistent with delayed onset of neutralization observed in the experimental Auger spectra.

We note that our model does not account for the possible role that the projected band gap of the underlying Au(111) may have on the ability of an ion to exchange charge in a way that is consistent with a jellium description of the metal. In particular, for perpendicular velocities below approximately 0.1 a.u. (2.2×10^5 m/s), which are present in the measurements of Refs. [9,10], it is predicted that deviations from the jellium description of charge exchange can arise for a bare substrate [34–36]. Although these time scale sensitive deviations were not derived for a thin film system, measurements sensitive to resonant charge exchange could be used to sense whether captured electrons originate from E_F or the LiF E_{vbm} and thus further distinguish the mechanisms and relevant time scales involved.

C. Al_2O_3/Co

Thin aluminum oxide films on cobalt was the experimental system studied in Ref. [12]. Al_2O_3 is considered a "high-k dielectric" with static permittivity of approximately $\epsilon = 8$

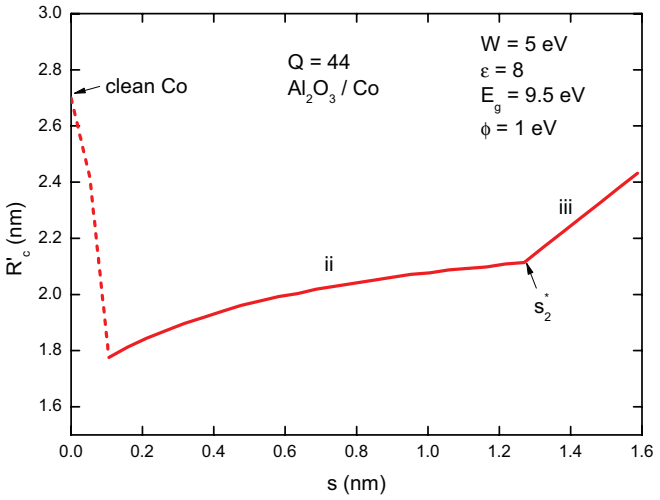

FIG. 10. (Color online) Thickness-dependent critical distances for $Q = 44$ interacting with Al_2O_3 films on Co. Vacuum limited transport from the metal (regime i) does not occur at any physically meaningful s due to relatively high ϕ and ϵ parameters. Instead, the barrier ϕ limits the capture of metal electrons and suppresses the capture distances R_c' (regime ii). The target appears to the HCI like a bulk dielectric beyond $s_2^* = 1.3$ nm.

(for plasma oxidized thin films [37]). The nominal band gap of bulk aluminum oxide ($E_g = 9.9$ eV) is smaller than that of bulk LiF. As with all materials fabricated as ultrathin films, the electronic properties are sensitive to preparation conditions, e.g., band gap differences may occur depending on whether plasma oxidation, thermal oxidation, or atomic layer deposition are used [38]. For plasma oxidized barriers, the energy difference between the metal Fermi energy and dielectric conduction band minimum was measured to be $\phi = 1$ eV [39]. This quantity can be determined by performing tunneling spectroscopy measurements of $Co/Al_2O_3/Co$ junctions. The Fermi energy lies within the band gap of the dielectric.

Figure 10 plots critical distance as a function of aluminum oxide film thickness, given the target parameters $E_g = 9.9$ eV, $\epsilon = 8$, $\phi = 1$ eV, and $W = 5$ eV. The charge state in the plot is $Q = 44$ (the highest charge state used in Ref. [12]). The dashed line from $s = 0$ to $s = 1$ represents how a robust ϕ is established almost immediately upon adding any dielectric. The high permittivity and the large difference between E_{vbm} and E_F result in a strong ϕ, so that even when $s = 0.1$ nm, the HCI has to approach much closer to extract the charge. The two distinct slopes in the solid $R_c'(s)$ line are regions ii (film limited capture from the metal) and iii (capture from the dielectric). The transition s_2^* occurs at a thickness of 1.3 nm.

Capture from the metal limited by the vacuum barrier does not occur within the range of thicknesses plotted. This means that the distance of first capture does not depend explicitly on the work function of the metal substrate in ultrathin films (when $s < s_2^*$). Instead, the barrier $\phi = E_{cbm} - E_F$ limits the capture of metal electrons. Also, for $s > 0$ nm, critical distance is suppressed compared to a clean Co target. R_c for the clean Co ($W = 5$ eV; $Q = 44$) from Eq. (5) is indicated at $s = 0$ nm in Fig. 10.

Although the capture distance is suppressed due to the presence of the film, the first captured electron can be expected to originate from the metal substrate behind the exposed dielectric film at thicknesses up to 1.3 nm. At thicknesses greater than 1.3 nm, the target begins to take on the properties of a bulk aluminum oxide target. Specifically, capture is limited by the high vacuum barrier between the valence band electrons in the aluminum oxide layer and the ion. These target electrons in the dielectric have an effective binding energy of $E_{vbm} = 13.9$ eV.

In the context of material modifications experiments [12], the prediction of above-surface capture of an electron from the metal may provide insight into damage mechanisms. If charge is removed from the metal instead of the dielectric film during above-surface neutralization, this suggests that modification of the thin film occurs upon ion impact as opposed to above surface.

TABLE I. Summary of critical distances at $Q = 36$ and $s = 1$ nm for three experimentally studied systems [9–12]. The regimes correspond to electron capture from the metal (vacuum limited) (i), electron capture from the metal (film limited) (ii), and electron capture from the dielectric film (iii). Parameters for each material system are displayed in the previous figures.

Film/substrate	R_c' (nm)	R_c (nm)	R_c'/R_c	(Regime) note
C_{60}/Au(111)	4.0	2.3	1.8	(i) enhancement
Al_2O_3/Co	1.9	2.4	0.8	(ii) suppression
LiF/Au(111)	0.9*	2.3	0.4	(iii) suppression
				*origin is $z = s$

D. Summary of experimental systems

The results of the model for the three material systems discussed in the previous section are summarized in Table I at film thickness $s = 1$ nm, and $Q = 36$. For C_{60} on Au(111), the 1 nm film increases the distance for the onset of neutralization. Neutralization starts with electrons in the metal (in the vacuum limited regime i). The relative enhancement of capture distance compared to the metal is $R_c'/R_c = 1.8$. In the Al_2O_3/Co system, capture still proceeds from the metal at 1 nm thickness, but the film slightly suppresses the capture distance by a factor $R_c'/R_c = 0.8$. The $s = 1$ nm film induces a film limited capture regime (regime ii). Here, R_c' is limited by the barrier ϕ within the dielectric and not the vacuum work function (W). In LiF/Au(111), a film thickness $s = 1$ nm blocks capture from the metal. The first captured electron comes from the valence band of the LiF film. In this case (region iii), the captured electron starts within the target at the position closer to the ion at a position s. Therefore, the distance between the ion and captured electron is $(R_c' - s)$. In comparing capture from the dielectric film to capture from the clean metal, we examine the ratio $(R_c' - s)/R_c = 0.4$. The asterisk in the table denotes this $R_c' \to (R_c' - s)$ correction that accounts for the initial position of the captured electron. In this comparison, we assume that the full bulk band gap $E_g = 14$ eV is present within the dielectric at all thicknesses. As discussed previously, the presence of a nonzero ϕ is required to explain the delayed onset of neutralization observed in the experiment [9].

V. SUMMARY

In summary, we presented an extension of the classical over-the-barrier model [1] to examine the first stage of neutralization for HCIs outside dielectric thin films on metals. Classical electrostatics were used to construct the potential profile for an "active electron" in a metal-dielectric-vacuum system in the presence of an HCI. The inclusion of a dielectric thin film leads to a significant modification of boundary conditions. The electron self-image was treated with the well-known dielectric continuum model. Over-the-barrier capture distances as a function of film thickness were obtained. We find that the first resonantly captured electron can be captured over the barrier either from filled states in the metal or dielectric, depending on the permittivity, band gap, and thickness of the film. Additionally, the thin film can either enhance or suppress the onset of neutralization. Within an $R_c'(s)$ plot, we observed the following qualitative structure:

(1) Regime i (vacuum limited): First captured electron comes from the metal. The onset of neutralization is enhanced with respect to the clean metal. This regime occurs for ultrathin films $s < s_1^*$ for low barrier heights ϕ and low permittivity values ϵ.

(2) Regime ii (dielectric film limited): First captured electron comes from the metal. The onset of neutralization can be either enhanced or suppressed, depending on ϕ and ϵ. R_c' is independent of the metal's vacuum work function, and instead depends on the barrier $\phi = E_{cbm} - E_F$. Regime ii occurs for thicknesses $s_1^* < s < s_2^*$.

(3) Regime iii (capture from dielectric): The dielectric film blocks the capture of metal electrons and suppresses the onset of neutralization when $s > s_2^*$. The film shields the metal electrons and the target behaves as a bulk dielectric, as described in Ref. [2].

Quantitative values of the transition thicknesses s_1^* and s_2^* are given for various high charge states in the systems C_{60}/Au(111), Al_2O_3/Co, and LiF/Au(111). The behavior of $R_c'(s)$ closely resembles the measured thickness-dependent enhancements in the relative emission yield reported in Ref. [11]. The model also predicts suppression for the onset of neutralization for LiF/Au(111), in agreement with the experiment [9] due to the large ϵ and as long as a nonzero ϕ exists, e.g., $E_{\text{gap}} > 7.5$ eV. An analysis of the Al_2O_3/Co system from Ref. [12] showed that for thin films ($s \approx 1$ nm), the first captured electrons originate from the metal.

ACKNOWLEDGMENT

R.E.L. and C.E.S. gratefully acknowledge financial support from NIST, Grant No. NSF-CHE-0548111, and Clemson University COMSET.

[1] J. Burgdörfer, P. Lerner, and F. W. Meyer, Phys. Rev. A **44**, 5674 (1991).
[2] L. Hägg, C. O. Reinhold, and J. Burgdörfer, Phys. Rev. A **55**, 2097 (1997).
[3] J. J. Ducrée, F. Casali, and U. Thumm, Phys. Rev. A **57**, 338 (1998).
[4] H. Kurz, F. Aumayr, C. Lemell, K. Toglhofer, and H. P. Winter, Phys. Rev. A **48**, 2192 (1993).
[5] H. Kurz, F. Aumayr, C. Lemell, K. Toglhofer, and H. P. Winter, Phys. Rev. A **48**, 2182 (1993).
[6] J. P. Briand, L. de Billy, P. Charles, S. Essabaa, P. Briand, R. Geller, J. P. Desclaux, S. Bliman, and C. Ristori, Phys. Rev. Lett. **65**, 159 (1990).
[7] J. Burgdörfer and F. Meyer, Phys. Rev. A **47**, R20 (1993).
[8] H. Winter, C. Auth, R. Schuch, and E. Beebe, Phys. Rev. Lett. **71**, 1939 (1993).
[9] H. Khemliche, T. Schlathölter, R. Hoekstra, R. Morgenstern, and S. Schippers, Phys. Rev. Lett. **81**, 1219 (1998).
[10] H. Khemliche, T. Schlathölter, R. Hoekstra, and R. Morgenstern, Phys. Rev. A **60**, 3800 (1999).
[11] E. Bodewits, R. Hoekstra, G. Kowarik, K. Dobes, and F. Aumayr, Phys. Rev. A **84**, 042901 (2011).
[12] R. E. Lake, J. M. Pomeroy, H. Grube, and C. E. Sosolik, Phys. Rev. Lett. **107**, 063202 (2011).
[13] R. E. Lake, J. M. Pomeroy, and C. E. Sosolik, Nucl. Instrum. Methods Phys. Res., Sect. B **269**, 1199 (2011).
[14] S. M. Sze and K. K. Ng, *Physics of Semiconductor Devices* (Wiley-interscience, New York, 2006).
[15] E. L. Wolf, *Principles of Electron Tunneling Spectroscopy* (Oxford University Press, Oxford, 2011).
[16] J. Burgdörfer, C. Reinhold, L. Hägg, and F. Meyer, Aust. J. Phys. 527 (1996).
[17] J. Burgdörfer, in *Atomic Collisions with Surfaces*, Chap. 11 (World Scientific, Singapore, 1993), p. 517.
[18] A. Bárány and C. J. Setterlind, Nucl. Instrum. Methods Phys. Res., Sect. B **98**, 184 (1995).
[19] P. J. Jennings and R. O. Jones, Adv. Phys. **37**, 341 (1988).
[20] C. B. Harris, N.-H. Ge, R. L. Lingle, J. D. McNeill, and C. M. Wong, Ann. Rev. Phys. Chem. **48**, 711 (1997).
[21] J. Gudde, W. Berthold, and U. Hofer, Chem. Rev. **106**, 4261 (2006).
[22] J. D. McNeill, J. R. L. Lingle, R. E. Jordan, D. F. Padowitz, and C. B. Harris, J. Chem. Phys. **105**, 3883 (1996).
[23] T.-C. Chiang, G. Kaindl, and T. Mandel, Phys. Rev. B **33**, 695 (1986).
[24] M. W. Cole, Phys. Rev. B **3**, 4418 (1971).
[25] J. D. Jackson, *Classical Electrodynamics*, 2nd ed. (Wiley, New York, 1975), Sec. 4.3.
[26] E. Durand, *Electrostatique: Méthods de Calcul Diélectriques*, Vol. III (Masson et Cie, Paris, 1966), Chap. 3, Sec. 2.
[27] M. Kleefstra and G. C. Herman, J. Appl. Phys. **51**, 4923 (1980).
[28] F. Schiller, M. Ruiz-Oses, J. E. Ortega, P. Segovia, J. Martinez-Blanco, B. P. Doyle, V. Perez-Dieste, J. Lobo, N. Neel, R. Berndt, and J. Kroger, J. Chem. Phys. **125**, 144719 (2006).
[29] S. L. Ren, Y. Wang, A. M. Rao, E. McRae, J. M. Holden, T. Hager, K. Wang, W.-T. Lee, H. F. Ni, J. Selegue, and P. C. Eklund, Appl. Phys. Lett. **59**, 2678 (1991).

[30] R. R. Zope, T. Baruah, M. R. Pederson, and B. I. Dunlap, Phys. Rev. B **77**, 115452 (2008).
[31] N. W. Ashcroft and N. D. Mermin, *Solid State Physics* (Holt, Rinehart and Winston, New York, 1976).
[32] D. Ochs, M. Brause, P. Stracke, S. Krischok, F. Wiegershaus, W. Maus-Friedrichs, V. Kempter, V. Puchin, and A. Shluger, Surf. Sci. **383**, 162 (1997).
[33] S. Pulm, A. Hitzke, J. Gunster, H. Muller, and V. Kempter, Radiat. Eff. Def. Solids **128**, 151 (1994).
[34] A. G. Borisov, A. K. Kazansky, and J. P. Gauyacq, Phys. Rev. Lett. **80**, 1996 (1998).
[35] T. Hecht, H. Winter, A. G. Borisov, J. P. Gauyacq, and A. K. Kazansky, Phys. Rev. Lett. **84**, 2517 (2000).
[36] L. Guillemot and V. A. Esaulov, Phys. Rev. Lett. **82**, 4552 (1999).
[37] S. Ruggiero and J. Barner, Z. Phys. B **85**, 333 (1991).
[38] J. Robertson, Eur. Phys. J.: Appl. Phys. **28**, 265 (2004).
[39] J. M. Pomeroy, R. E. Lake, and C. E. Sosolik, Nucl. Instrum. Methods Phys. Res., Sect. B **269**, 1238 (2011).